

LINEAR MATHEMATICAL MODELS FOR WELDS IN LASER WELDING

Remus BOBOESCU¹

¹ Ph.D., Professor, Polytechnic University Timișoara

Abstract. It presents a study on the molten area produced at irradiation of steel plates with laser beam. A full factorial experimental design type 2³ is used to evaluate the effects of power, welding speed and defocus (the distance between the focal plane and the surface of the piece). Parameters effects on the measured sizes for the weld cross section and the weld surface are presented by linear polynomial models. We discuss the variations presented by Pareto diagrams and response surfaces. It presents statistical analysis of the parameters effects by ANOVA method. It shows that the first effect on the analyzed sizes is given power. Identify the dynamic aspects of the welding process associated with keyhole welding regime.

Keywords: laser welding, weld cross section, full factorial design, welding pool.

1. INTRODUCTION

Laser welding has two distinct regimes, conduction welding regime and keyhole welding regime which differ in the weld penetration and weld cross section shape.

Conduction welding regime. This regime is called conduction limited welding. The solid-liquid interface heat transfer mechanism is exclusively by conduction. Heat is conducted directly from the heat source that occurs due laser radiation from the workpiece surface within the material. Conduction welding regime is characterized by irradiation sufficient to produce piece surface melting and vaporization but not enough to produce vaporization in the depth of material. For conduction welding regime values of F ratio between the weld width and weld depth are higher than 1, $F \geq 1$. As an indicative value for the weld depth in conduction regime is 1.5 mm [1]. Defects that are obtained in conduction welding regime are cracks on the weld surface.

Keyhole welding regime. This welding regime involves the keyhole phenomenon in weld pool which involves

the values of laser beam intensities that exceed threshold needed to produce a vapor front propagation in the material. Heat transfer mechanism at solid-liquid interface involves both conduction and convection due to the melt movement in the weld pool. In weld cross section there is a welding defects gas bubbles, the presence of this pore led to the designation of keyhole regime (“key hole”). F ratio between weld width and weld depth has a smaller value than 1, $F \leq 1$. Defects in welds are obtained for the keyhole welding regime are gas porosity due to dissolution into the melt a gas bubbles and vacuum large areas. The presence of the Keyhole and vapor within the material made pushing melting front (solid-liquid interface) inside the material. This provides increased weld penetration [2], [3], [4]. Plate with made welds and particular aspects of welds cross-section and weld surface are shown in Figure 1.

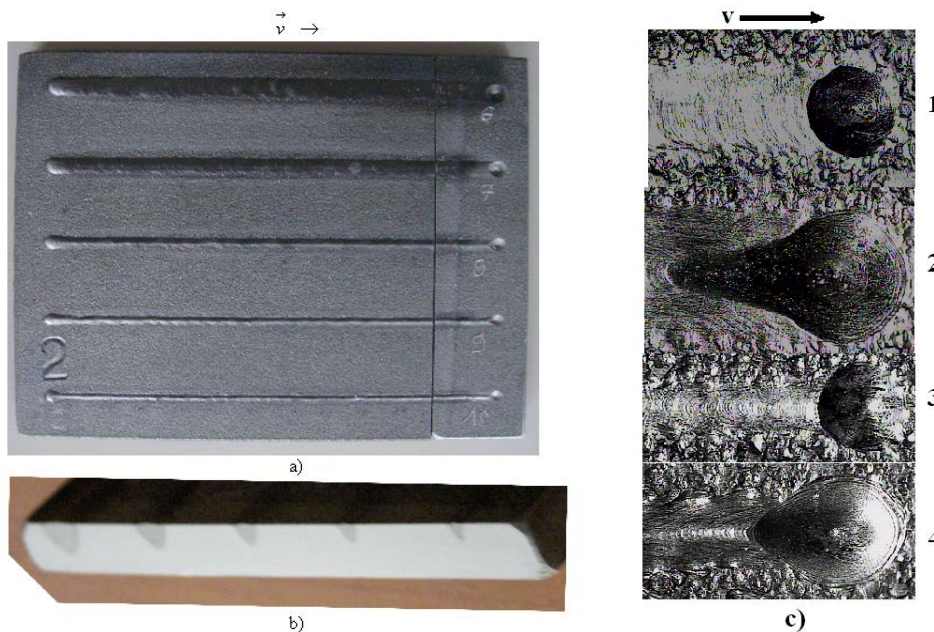


Figure 1 Picture of welds a) plate surface with welds , b) cross section through the welds, c) crater at the end of the weld for defocus at piece surface

The paper proposes a study of the molten zone is obtained in material at laser beam welding. It looks like those in characterizing keyhole regime occurs sizes associated with both weld cross section and weld surface. Experimental factorial design 2³ used presents for higher levels of power keyhole welding regime and for the lower power level presents the conduction welding regime. It will discuss variation of the

response functions relative to varied parameters power and welding speed. Distance between workpiece surface and the laser beam focal plane is called defocusing (defocusing depth or defocus) figure 2. Defocus effect will be compared with effects of power and welding speed. Defocus variation done the particular situations for keyhole regime. Defocus is

therefore appropriate to consider as a parameter for a factorial experimental design.

Mathematical modeling was performed using Statgraphics program. The main discussion is conducted on

2. EXPERIMENTAL PROCEDURE

The material used was steel Dillimax500 EN 10137. This is a fine grain steel with high elasticity limit elasticity. Chemical composition with upper limit expressed as a percentage is given as follows : $C \leq 0.16$, $Si \leq 0.5$, $Mn \leq 0.16$, $P \leq 0.02$, $S \leq 0.01$, $Cr \leq 0.7$, $Ni \leq 1$, $Mo \leq 0.6$, $V+Nb \leq 0.08$.

The experiment consisted of fusion lines (welds) with the line length of 110mm on steel Dillimax500 plates with 10 mm thickness. An industrial laser machine Nd: YAG Triumph Haas 3006D was used. It emits radiation with wavelength $\lambda = 1.06 \mu\text{m}$ and have a maximum power of 3kW.

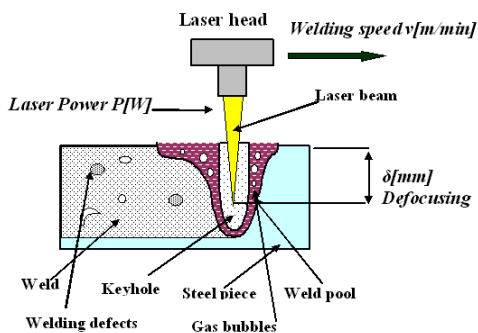


Figure 2: Schematic diagram of the laser welding process

After the welding the plates were cut. Cutting of plates was performed at 20 mm before the end of the process, in stable part of weld, at same distance for all welds. The piece section has been metallographic processed (polishing and acid attack using Nital) to obtain images of melted metal, heat affected zone (HAZ), and microstructure. On the metallographic processed section were made measurements of the weld width w [mm] and weld depth h [mm] using a microscope to study with accuracy of 0.1 mm. Molten zone

the effects of the parameters presented by Pareto diagrams. Experimental data analysis procedure was similar to that used in [5] and [6].

Irradiation was performed in continuous regime. Laser beam was transmitted through a fiber with 0.6 mm diameter. The focusing system assures the spot in focal point with 0.6 mm diameter. The focal distance of lens was 200 mm. As protective gas was argon with a flow rate of 20 l/min. The welds were made on the sheets of material with $100 \times 130 \times 10$ mm dimensions. There was a space 20 mm between two consecutive welds. The radiation was controlled by variation of three parameters: laser power, welding speed and defocusing, figure 2.

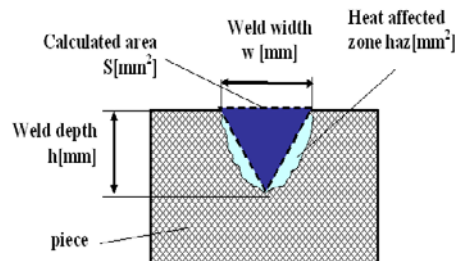


Figure 3: Schematic diagram of weld cross section

area was measured using a millimeter scale of precision 1 mm² on the weld cross-section, figure 3.

The experimental plan used was one of complete factorial. To achieve mathematical models and statistical analysis of variations was used Statgraphics program.

For this analysis has introduced a dimensionless parameter values. Both systems will be used for the presentation of mathematical models. Experimental plan is presented in Figure 4

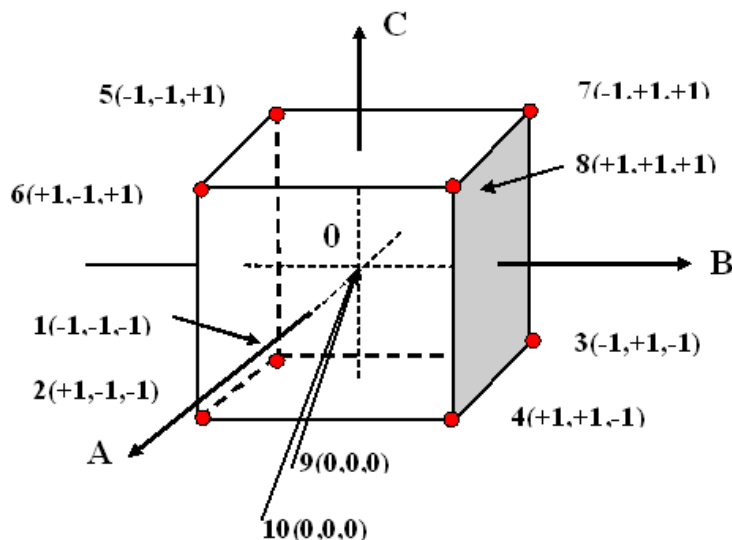


Figure 4 Scheme for experimental design type 2³ for Power $A = P - 2$ [-], Welding speed $B = -2.33 + 2.22v$ [-], Defocusing $C = -1 - \delta$ [-]

3. WELD CROSS-SECTION ANALYSIS

Calculated area S [mm^2] of weld cross-section is a direct result of measuring the weld width w [mm] and weld depth h [mm]. Calculated area shows „interaction” between the two measured quantities directly as a function of their product. Calculated area S is given by:

$$S = \frac{1}{2} w \cdot h \text{ [mm}^2\text{]}$$

(1)

The mathematical model for calculated area S is given by (2). Statistical analysis of the variations is given in the table 1.

$$S = 4.403 + 3.7275 A - 1.88 B - 0.03 C \text{ [mm}^2\text{]}$$

(2)

Figure 6 shows the Pareto chart for the calculated area S . It is noted that the area S increases with power and

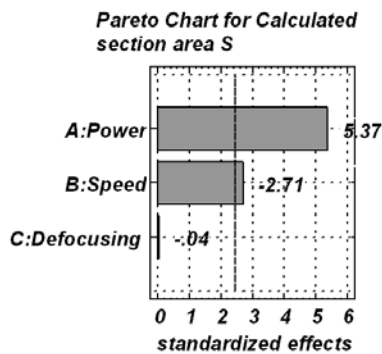


Figure 6 Pareto Chart for calculated weld cross-section area

Figure 8 shows variation of S calculated area with power and defocus. It is noted that on the experimental field area S increases with power. Defocus does not produce significant variations. To achieve the welded joints is recommended that the melting zone to be extended. It is recommended for high values of power but not the maximum value. Figure 9 presents the response surface for calculate area S function of welding speed and defocus. It is noted that on the experimental field calculated area S decreases with speed and does not vary with defocus. It is recommended for relatively low values for welding speed.

On the weld cross section heat affected zone is marked in the material by changing the structure. Heat affected zone haz [mm^2] contains the molten and resolidified areas. Heat affected zone is marked by isothermal line under melting temperature. Heat affected zone area was obtained by

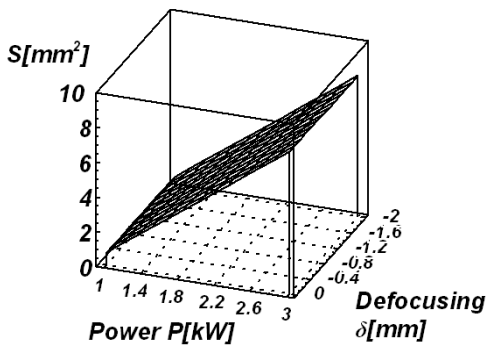


Figure 8 Response surface for calculated weld cross-section area with power and defocusing

decreases with welding speed. The effects of power and speed were statistically significant. The effect of power is much greater than the welding speed effect. It looks like the size of molten zone can be controlled by power. Defocus effect is small and not statistically significant. Defocus decreases calculated area S . Calculated area is heavy reliance on power and exclude almost defocus variations.

Figure 7 shows the surface response for calculated area S on weld cross-section with power and welding speed. It shows that the on the experimental field calculated area increases with power and decreases with welding speed. The effect of power was much greater than the welding speed effect is shown that there can vary widely welding speed without changing much weld cross section. From this is possible to optimize the welding process by increasing the welding speed.

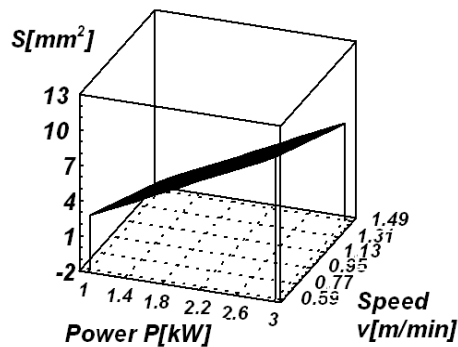


Figure 7 Response surface for calculated weld cross-section area with power and speed

direct measurement on the weld cross section. Measuring the size was more accurate than the melted area.

The mathematical model for heat affected zone area is given by (3).

$$haz = 9.75 + 7.5A - 3.875B - 0.125C \text{ [mm}^2\text{]} \quad (3)$$

Figure 10 shows the Pareto chart for the area of heat affected zone. It is noted that the area of heat affected zone increases with power with and decreases welding speed. The first, highest, effect is the power effect and the second effect is the welding speed. The effects of welding power and speed were statistically significant. Defocus effect is small compared with other effects. Defocus increases heat affected zone area. It looks like that for the heat affected zone area the main effect is power effect. It shows that the thermal material behavior can be best controlled by power.

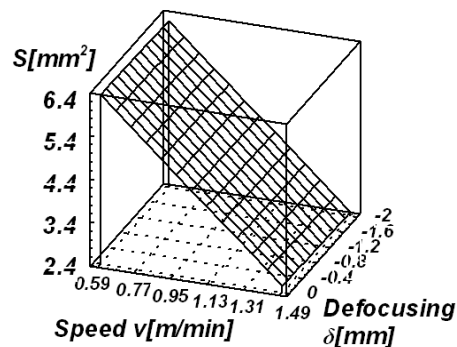


Figure 9 Response surface for calculated weld cross-section area with speed and defocusing

Figure 11 presents response surface for heat affected zone area with power and welding speed. It is noted that the on experimental field heat affected zone area increases with power and decreases with welding speed. Maximum values are obtained at high power and low welding speed. In this case there is a large melted area. It is noted that there may be increased welding speed without lowering the heat affected zone area. By increasing the welding speed is achieved optimizing the welding process.

Figure 12 shows changes in heat affected zone area

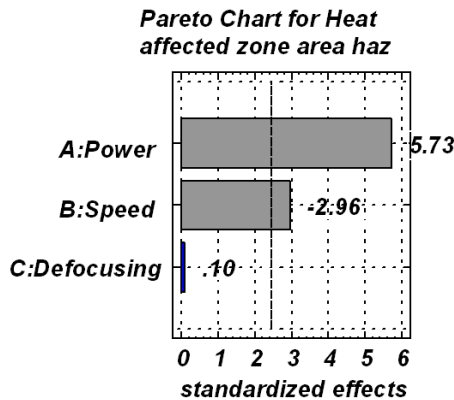


Figure 10 Pareto Chart for heat affected zone area

with power and defocus. It is noted that on the experimental field heat affected zone area increases with power. Defocus does not produce variations. It is recommended to use high values for power and laser beam focus within the piece.

Figure 13 presents response surface for heat affected zone area with defocus and welding speed. It is noted that on the experimental field the heat affected zone area decreases with speed. Defocus does not produce significant changes on heat affected zone area. It is recommended to not use high welding speeds.

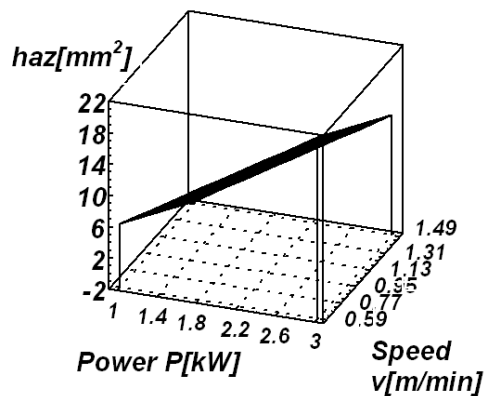


Figure 11 Response surface for heat affected zone area with power and speed

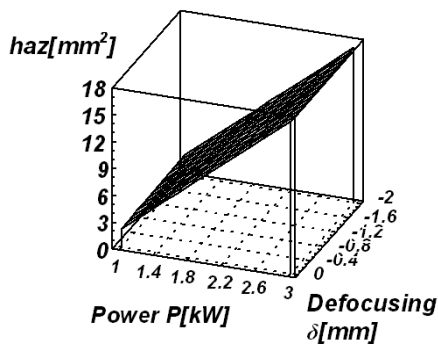


Figure 12 Response surface for heat affected zone area with power and defocusing

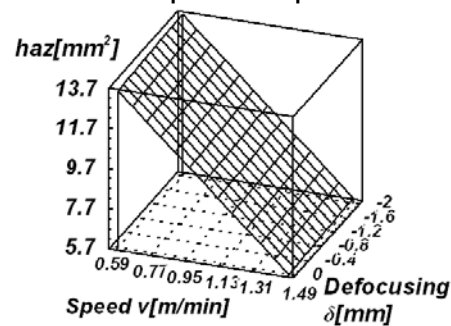


Figure 13 Response surface for heat affected zone area with speed and defocusing

4. WELD SURFACE ANALYSIS

The mathematical model for weld width is given by (4). Statistical analysis of variance effects ANOVA method is presented in Table 2.

$$L = 2.034 + 0.5825A - 0.46B + 0.0075C \text{ [mm]} \tag{4}$$

Table 1 ANOVA for calculated area S on weld cross-section

Effect	Sum of Squares	DF	Mean. Sq.	F-Ratio	P-val
A(power)	111.154	1	111.154	28.88	0.001
B(speed)	28.275	1	28.275	7.35	0.035
C(defocusing)	0.007	1	0.007	0.00	0.967
Total error	23.092	6	3.848		
Total (corr)	162.529	9			
$R^2 = 0.85$		$R^2(\text{adj. for d. f.}) = 0.78$			

Table 2 ANOVA for weld width L

Effect	Sum of Squares	DF	Mean. Sq.	F-Ratio	P-val
A(power)	2.714	1	2.714	9.22	0.02
B(speed)	1.692	1	1.692	5.75	0.05
C(defocusing)	0.0004	1	0.0004	0.00	0.97
Total error	1.767	6	0.294		
Total (corr)	6.175	9			
$R^2 = 0.71$		$R^2(\text{adj. for d. f.}) = 0.57$			

In Figure 15 is presented Pareto diagram for weld width L. It is noted that the weld width increases power and decreases with the welding speed. The effects of power and welding speed were statistically significant. Defocus effect is small and has not an important contribution to establishing the weld width. It shows that the weld width is controlled mainly by

power. Figure 16 presents response surface for the weld width variation with power and welding speed. It is noted that on the experimental field weld width increases with power and decreases with welding speed. Maximum values of weld width are obtained at maximum power and minimum welding speed.

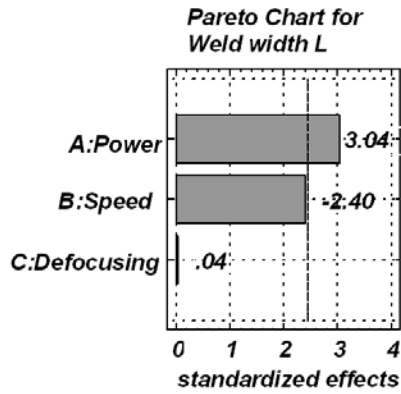


Figure 15 Pareto Chart for weld width

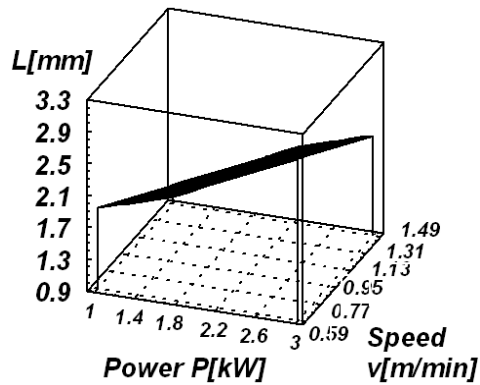


Figure 16 Response surface for weld width with power and speed

When stopping laser irradiation in the material remains a crater. This is a trace of the weld pool. Was measured the

crater area and three linear dimensions to characterize the shape and deformation of the crater.

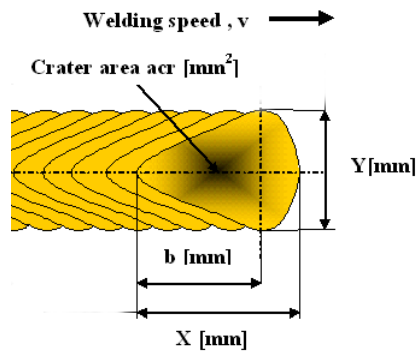


Figure 17 Sizes measured for at the crater end of the weld

The mathematical model for crater area is given in relation (5). Statistical analysis of variations by ANOVA method is presented in Table 3.

$$acr = 10.017 + 6.885A + 2.2225B + 0.665C \text{ [mm}^2\text{]} \quad (5)$$

In Figure 18 is presented for Pareto diagram the crater area. It is noted that the crater area increases with power, welding speed and defocus. By increasing the power increases the amount of melt thus weld pool surface area represented by the crater area. By increasing the welding speed is reduced vaporization and favors melting which will lead to an increase in the crater area.

Defocus increases the laser beam spot area at piece surface. Thus, increases the weld pool surface and therefore the crater area. Power effect is statistically significant. It shows that the weld dimensions are given by the effect of power. Effects of defocus and welding speed although lower than that of power had an important contribution.

Response surface in Figure 19 shows the variation of the crater area with power and welding speed. It is noted that on the experimental field of the crater area increases with power and with welding speed. Increased with power is stronger than increased with welding speed, situation useful for optimizing welding process.

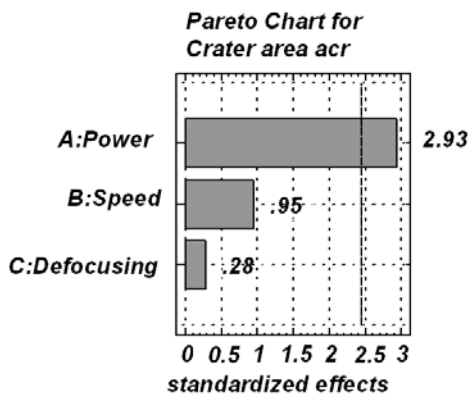


Figure 18 Pareto Chart for crater area

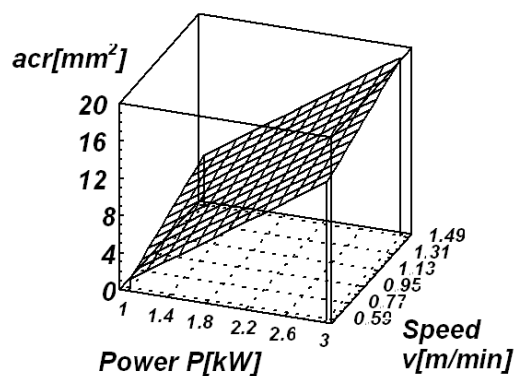


Figure 19 Response surface for crater area with power and speed

Deviation from circularity was determined by comparing the transverse and longitudinal dimensions of the crater. Crater elongation was measured from the center of the crater at the back of it (opposite direction of welding speed).

The front of the crater was considered semi-circular shape with radius r [mm]. Elongation was compared with the radius of circular part of the crater.

Crater size (X axis in the direction of welding, transverse axis Y and elongation b) and its area was measured indirectly using images of the crater, figure 2. Crater depth was measured using a comparator. Weld width, crater dimensions X, Y, b , crater area and the crater depth are measured sizes. Deviation from circular and crater volume are calculated sizes. They are given by the following relations:

- for deviations from circularity:

$$abc = \frac{b - r_{med}}{r_{med}} [\%] \quad (6)$$

$$\text{where: } r_{med} = \frac{1}{2} \left(\frac{Y}{2} + X - b \right) [\text{mm}] \quad (7)$$

The mathematical model for the deviation from circularity is presented by relation (8). Statistical analysis of variances by ANOVA method is presented in Table 4.

$$abc = 57.16 + 45.9625A - 16.1625B - 16.2375C [\%] \quad (8)$$

In Figure 20 is presented Pareto diagram for the deviation from circularity for shape of crater obtained at the end of the welding process. Deviation from circularity strong increases with power. Power effect is statistically significant.

Table 3 ANOVA for crater area acr

Effect	Sum of Squares	DF	Mean Sq.	F-Ratio	P-val
A(power)	379.225	1	379.225	8.59	0.02
B(speed)	39.516	1	39.516	0.90	0.39
C(defocusing)	3.537	1	3.537	0.80	0.78
Total error	264.737	6	44.122		
Total (corr)	687.012	9			
$R^2 = 0.61$		$R^2(\text{adj. for d. f.}) = 0.42$			

Table 4 ANOVA for circularity deviation crater abc

Effect	Sum of Squares	DF	Mean Sq.	F-Ratio	P-val
A(power)	16900.411	1	16900.4	19.64	0.004
B(speed)	2089.811	1	2089.8	2.43	0.17
C(defocusing)	2109.251	1	2109.2	2.45	0.168
Total error	5162.390	6	860.3		
Total (corr)	26261.864	9			
		$R^2(\text{adj. for d. f.}) = 0.70$			

The second effect is the effect of defocus. Defocus and welding speed effects lower the deviation from circularity.

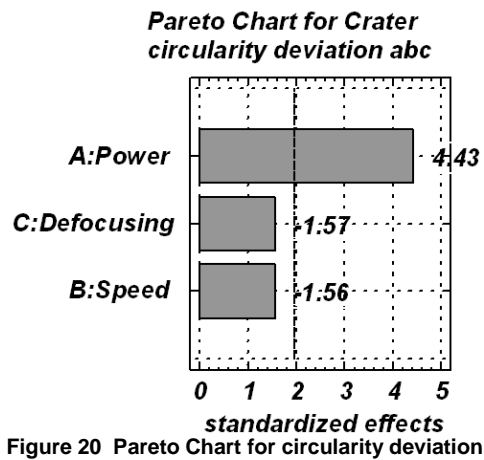


Figure 20 Pareto Chart for circularity deviation

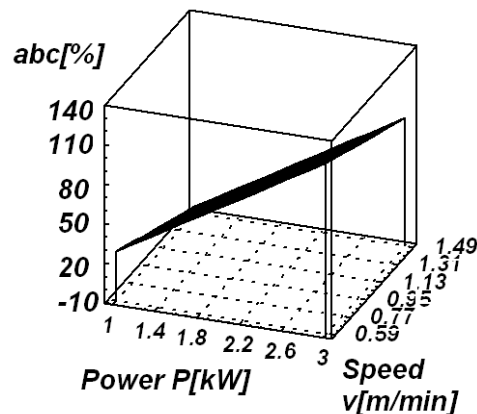


Figure 21 Response surface for circularity deviation with power and speed

Defocus increases the laser beam spot size at piece surface, it reduces the deformation of the weld pool. Increasing the welding speed decreases the time of interaction between laser beam and material, thus decreases the melt movement in the welding bath. On the overall effect of keeping the circular shape of the crater given by defocus and speed is less than deformation of the crater effect given by the power.

Figure 21 presents response surface for deviation from circular with power and welding speed. Deviation from circularity increases with power. Increasing deviation from circularity shows transition from the conduction welding regime to keyhole welding regime.

5. CONCLUSIONS

On irradiation with laser beam for high levels of intensity material melting occurs. Melted zone size in material determines how the laser beam can be used for welding of metallic materials. Depending on the laser beam intensity level was identified welding regime by conduction and keyhole

welding regime. There have been made welds (fusion lines) after a factorial experimental plan type 2^3 . Has been shown to characterize the molten zone is necessary analysis of weld cross-section and weld surface, several sizes were analyzed for them. Varied parameters in experiments were power, welding speed and defocus.

There has been made linear mathematical models. Parameters effects were shown following:

- Linear models for welds made with laser shows the role each of the varied parameters even if accuracy by the correlation coefficient given is sometimes low.
- Size measured in conditions close show the same type of variation.
- The main effect on measured quantities it has power.
- Power has a effect of increasing sizes of melted zone and welding speed of melt has a effect of decreasing sizes of melt zone.

**“Mircea cel Batran” Naval Academy Scientific Bulletin, Volume XIV – 2011 – Issue 1
Published by “Mircea cel Batran” Naval Academy Press, Constanta, Romania**

-Defocus has little effect on quantities that characterize the weld cross section but considerable effect on quantities that characterize weld surface.

Mathematical models presented in the paper are

useful for determining the size of the melted zone in material and thereby to achieve the laser beam welds. Deformation of the crater shows melt movement in welding bath. Increase of power produces increased of melt movement in welding bath.

REFERENCES

- [1] Alexander F. H. Kaplan, Masami Mizutani, Seiji Katayama, Akira Matsunawa, “Keyhole Laser Spot Welding”, *International Conference Applications of Lasers and Electro-Optics* 2002
- [2] Yukimichi Sasaki, Tadashi Misu, Shunro Yoshioka, and Toshiyuki Miyazaki, “Monitoring of YAG Laser Spot Welding-Detection of Porosity Defect by Acoustic Signal” *International Conference Applications of Lasers and Electro-Optics* 2002.
- [3] Inoue, Miamoto, Ono, Adachi, Matsumoto, “In process monitoring of penetration depth in 20 class CO₂ laser welding of thick sections” *International Conference Applications of Lasers and Electro-Optics* 1999
- [4] .Jae Y. Lee, Sung H. K., Dave F. Farson, Choong D. Yoo, “Mechanism of keyhole formation and stability in stationary laser welding”, *J. Phys. D: Appl. Phys.* 35 (2002) 1570–1576.
- [5] G. Casalino b, K.Y. Benyounis, M.S.J. Hashmi “An ANN and Taguchi algorithms integrated approach to the optimization of CO₂ laser welding” *Advances in Engineering Software* 37 (2006) 643–648
- [6] K.Y. Benyounis, A.G. Olabi, M.S.J. Hashmi “Optimizing the laser-welded butt joints of medium carbon steel using RSM” *Journal of Materials Processing Technology* 164–165 (2005) pp:986–989.